Angewandte
International Edition Chemie

Sensors

DOI: 10.1002/anie.201204373

Room-Temperature Hydrogen Sensing with Heteronanostructures Based on Reduced Graphene Oxide and Tin Oxide**

*Patrícia A. Russo, Nicola Donato, Salvatore Gianluca Leonardi, Seunghwan Baek, Donato E. Conte, Giovanni Neri, and Nicola Pinna**

Hydrogen is used in many industrial processes and is regarded as one of the most promising clean-energy carriers for future applications in transportation and power generation.[1] However, it is also a highly flammable gas and explosive when mixed with air at volume concentrations higher than about 4%; consequently, hydrogen manipulation requires constant monitoring for leaks. There are several types of H_2 sensors commercially available or in development, but the prospect of the widespread use of hydrogen as a fuel in the near future would require sensors that are highly sensitive, accurate, durable, small in size, and easy to fabricate, with short response and recovery times and low power consumption. None of the sensors presently available can fulfill all these requirements simultaneously.[2,3]

Metal-oxide semiconductors, such as SnO_2, are widely used as sensing layers for the detection of gases, including hydrogen, owing to their high sensitivity, fast response and recovery, stability, small size, simplicity, low cost, and simple interface electronics.[4,5] However, one significant disadvantage of sensors of this type is the high temperatures necessary for their operation (usually well above 200°C),[6] which increase the power consumption of the device. Hence, if the operating temperature of sensors based on semiconductor metal oxides could be decreased considerably without compromising other important aspects of their performance, such as sensitivity or response and recovery times, the potential of these sensors for widespread application would be improved significantly.

Different strategies have been employed to enhance the performance of semiconductor metal oxides in H_2 sensing, including the fabrication of 1D nanostructures (i.e. nanotubes, nanowires, and nanorods)[4,7–11] and the combination of the metal oxides with organic or carbon nanomaterials.[12–16] In particular, the incorporation of carbon nanostructures, such as carbon nanotubes (CNTs) or graphene, in H_2-sensing devices seems to be a promising approach, owing to the unique electronic and structural properties of these materials. Several different types of H_2 sensors with enhanced performance at low temperature have been reported previously, including optical sensors[17] and field-effect-transistor devices, such as those developed by Janata, Doll, Eisele, and coworkers.[18,19] However, in this study, we focused essentially on resistive H_2 sensors based on carbon nanostructures. Tin oxide/carbon nanotube nanocomposites have performed well in the past in terms of their operating temperature,[13,14] response times,[12,14] or sensitivity.[12] The properties of graphene have also been explored for the detection of hydrogen.[20–28] In addition to its high electronic conductivity, graphene has a very large theoretical surface area (twice as high as that of multiwalled carbon nanotubes) and shows structural flexibility and low electrical noise as a result of its crystal lattice and 2D nature: properties that are extremely desirable for gas-sensing applications.[29] However, pure graphene is not sensitive to hydrogen.[30] Therefore, most of the resistive hydrogen sensors based on graphene that have been reported so far consist of graphene layers functionalized with Pd or Pt nanoparticles and films, as it is well-known that these metals interact selectively with hydrogen molecules and catalyze their dissociation.[20,31] The use of nanocomposites based on metal oxides and graphene as hydrogen-sensing layers is, on the other hand, relatively unexplored.

Herein, we report on the hydrogen-sensing performance of nanostructures fabricated from reduced graphene oxide (RGO), tin oxide, and platinum by simple, fast, and readily scaled up microwave-assisted methods. The SnO_2/RGO and Pt–SnO_2/RGO nanostructures showed enhanced sensing performance relative to that of the corresponding pure and binary systems as a consequence of synergistic effects between the different components in the composites. In particular, the Pt–SnO_2/RGO sensor can detect H_2 even at

---

[*] Dr. P. A. Russo, Dr. D. E. Conte, Prof. N. Pinna
Department of Chemistry, CICECO, University of Aveiro
3810-193 Aveiro (Portugal)
Dr. N. Donato
Department of Matter Physics and Electronic Engineering
University of Messina, 98166 Messina (Italy)
Dr. S. G. Leonardi, Prof. G. Neri
Department of Industrial Chemistry and Materials Engineering
University of Messina, 98166 Messina (Italy)
S. Baek, Prof. N. Pinna
World Class University (WCU) program of Chemical Convergence for Energy & Environment (C2E2)
School of Chemical and Biological Engineering
College of Engineering, Seoul National University (SNU)
Seoul, 151-744 (South Korea)
Prof. N. Pinna
Humboldt-Universität zu Berlin, Institut für Chemie
Brook-Taylor-Strasse 2, 12489 Berlin (Germany)
E-mail: nicola.pinna@hu-berlin.de

[**] This research was supported financially by the WCU (World Class University) program through the National Research Foundation (NRF) of Korea, which is funded by the Ministry of Education, Science and Technology (R31-10013), and by Fundação para a Ciência e a Tecnologia (FCT) projects PTDC/CTM/098361/2008 and SFRH/BPD/79910/2011. Regina Rothe from the Max Planck Institute of Colloids and Interfaces is acknowledged for N_2-adsorption measurements.

Supporting information for this article is available on the WWW under http://dx.doi.org/10.1002/anie.201204373.

room temperature with high sensitivity. Furthermore, this sensor is able to respond in 3–7 s and recover in 2–6 s, depending on the hydrogen concentration.

Graphene oxide (GO) was prepared from graphite by a modified Hummers method.[32] GO was first coated with SnO_2 nanoparticles in a microwave-assisted synthesis in benzyl alcohol; $SnCl_4$ was used as the metal-oxide precursor.[33] Platinum nanoparticles were subsequently deposited onto the SnO_2/RGO structure by the reduction of $[H_2PtCl_6]$ in ethylene glycol at 140 °C for 5 min with the aid of microwave radiation. The nominal weight percentage of the carbon, tin oxide, and platinum components on the Pt–SnO_2/RGO nanocomposite was 24, 56, and 20 %, respectively. Pure SnO_2 nanoparticles, GO reduced in benzyl alcohol (RGO), and Pt/RGO were prepared according to procedures described in the experimental section of the Supporting Information.

To gain insight into the growth mechanism of the tin oxide nanoparticles on the graphene oxide surface, we analyzed the reaction solution by ^{13}C and ^{1}H NMR spectroscopy (see Figure S1 in the Supporting Information). It was possible to identify not only benzyl alcohol ($\delta_C = 65.33$ ppm, $-CH_2-$) but also benzyl ether ($\delta_C = 72.07$ ppm, $-CH_2-$) in the final reaction mixture. A similar result was obtained for the $SnCl_4$/benzyl alcohol system in the absence of the carbon support.[34] Makowski et al.[34b] found that SnO_2 nanoparticles prepared from tin chloride in benzyl alcohol catalyzed the conversion of benzyl alcohol into benzyl ether; benzyl chloride was an intermediate of the reaction. Therefore, the growth of the SnO_2 nanoparticles on the RGO surface seems to proceed through an alkyl halide elimination in which benzyl chloride and HCl are also formed.[35] The particles then catalyze the formation of benzyl ether from benzyl alcohol and benzyl chloride.[34b]

The X-ray diffraction patterns of the sensing materials investigated are shown in Figure S2 of the Supporting Information. As expected, pristine GO exhibits a very intense and broad reflection centered at 12.878 2θ°. Relative to the 002 reflection of pure graphite, a significant shift towards lower angles is observed. As reported in the JCPDS file #04-014-0362, the 002 reflection appears at 26.375 2θ°; thus, GO sheets are considerably further apart from one another than in crystalline graphite ($d_{002} = 0.687$ nm for GO and $d_{002} = 0.335$ nm for graphite). This effect is generally attributed to the presence of superficial oxygen functional groups and H_2O molecules in between the GO layers.[36] On the other hand, in the XRD pattern recorded for the RGO obtained after treatment in benzyl alcohol, this peak is broader and appears at 26.69 2θ°; increased background intensity is also observed. It was shown previously[33,37] that alcohols act as reducing agents of graphene oxide. The broad peak in the RGO pattern indicates that GO was partially reduced by benzyl alcohol and is significantly exfoliated.[36] Further evidence for the exfoliation of the RGO was provided by the BET surface areas of the final SnO_2/RGO composites of around 130 $m^2 g^{-1}$, as calculated from the nitrogen-adsorption isotherms (see Figure S3), and the absence of a reflection corresponding to the stacking of GO in the powder XRD pattern. The XRD patterns of tin oxide, SnO_2/RGO, and Pt–SnO_2/RGO exhibit the typical peaks of the SnO_2 cassiterite structure. The XRD pattern of Pt–SnO_2/RGO also shows the 111, 200, and 220 reflections of the face-centered-cubic platinum lattice and thus confirm the presence of both nanoparticle types in this heterostructure (see Figure S2). The sizes of the SnO_2 and platinum nanoparticles, as estimated on the basis of the Scherrer equation, are 3–5 nm and 3 nm, respectively.

Figure 1 shows TEM and high-resolution TEM (HRTEM) images of the SnO_2 nanoparticles and SnO_2/RGO heterostructure. The SnO_2 nanoparticles synthesized in the absence of GO are well-dispersed on the TEM grid and show a homogeneous particle size of approximately 5 nm (Figure 1 a), in agreement with our estimations based on the XRD data. SnO_2 nanoparticles of a similar size were formed at the surface of the RGO (Figure 1 b). They show well-defined lattice fringes in the HRTEM image (Figure 1 c). The power spectrum (PS) of this HRTEM image shows sharp spots due to the 5 nm SnO_2 nanoparticles (Figure 1 d). The first two families of spots (two circles drawn) are due to the 110 and 101 reflections of the SnO_2 cassiterite structure.

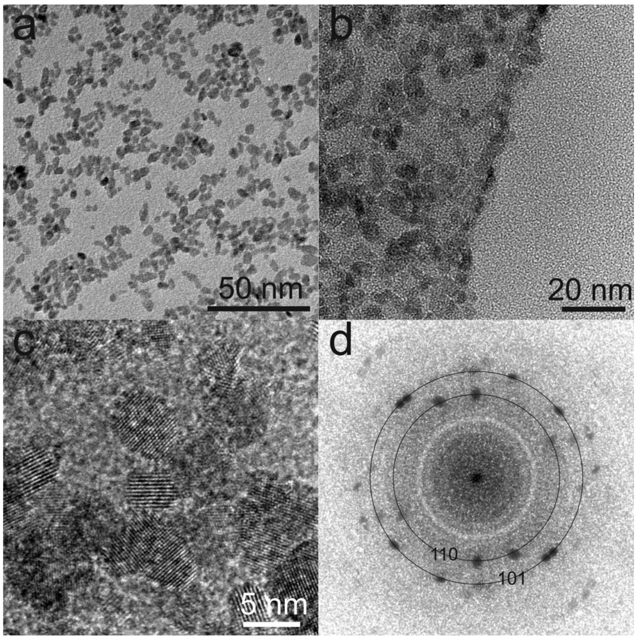

Figure 1. a) TEM image of SnO_2. b) TEM image of SnO_2/RGO. c) HRTEM image of SnO_2/RGO. d) PS of the whole HRTEM image in (c).

The TEM and HRTEM images of Pt–SnO_2/RGO (Figure 2 a,b) show an edge of an RGO sheet covered by a dense monolayer of Pt and SnO_2 nanoparticles. The nanoparticles exhibit well-defined lattice fringes, which indicate their high crystallinity. To assess the homogeneous distribution of the metal oxide and metal nanoparticles, we subjected the HRTEM images to Fourier filtering. The power spectrum (PS) of the whole HRTEM image in Figure 2 b shows the typical reflections of SnO_2 and Pt (Figure 2 c). For example, the spots marked with blue and yellow circles are the 110 and 101 reflections of SnO_2, and the spots marked in red are due to Pt 111. Fourier filtering of the HRTEM image selecting

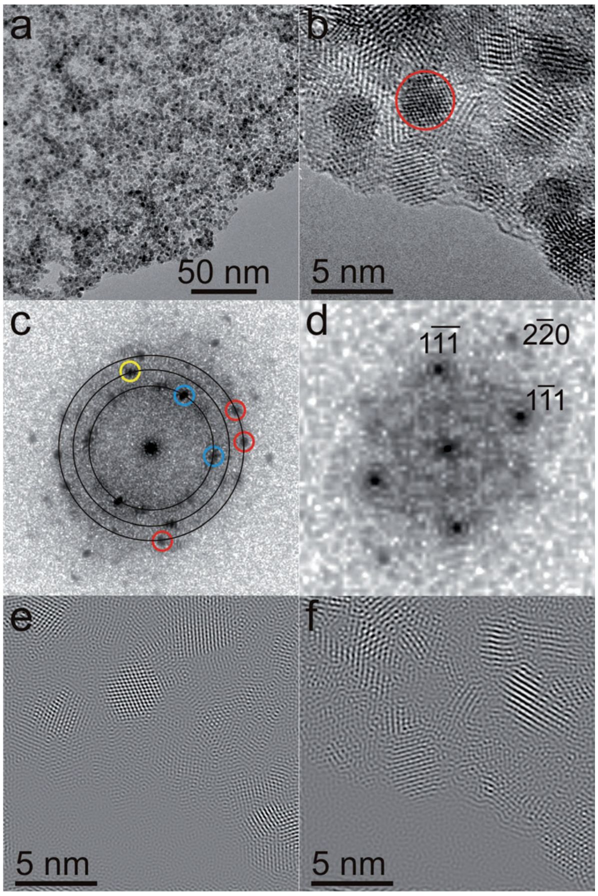

Figure 2. a) TEM and b) HRTEM images of Pt–SnO_2/RGO. c) PS of the whole HRTEM image. d) PS of the region of the HRTEM image indicated by the red circle. e) Fourier-filtered image acquired from the HRTEM image by using the 111 reflections of Pt. f) Fourier-filtered image acquired from the HRTEM image by using the 110 and 101 reflections of SnO_2.

only the 111 reflections of Pt or the 110 and 101 reflections of SnO_2 are shown in Figure 2e and f, respectively. The regions in which lattice fringes are visible denote the position of crystallographically well oriented Pt and SnO_2 nanoparticles. The results show that the two nanoparticles were distributed homogeneously on the RGO support. For example, the PS of the region marked in red in the HRTEM image is characteristic of a single crystalline 3 nm Pt nanoparticle oriented along the [110] direction (Figure 2d).

To assess the potential of the SnO_2/RGO and Pt–SnO_2/RGO heterostructures for the fabrication of resistive hydrogen sensors, we investigated their H_2-sensing properties at low temperature (see Figure S4). Pt–SnO_2/RGO was able to detect the lower hydrogen concentration tested (0.5%) with good sensitivity even at room temperature (25°C). However, we set the operating temperature at 50°C to avoid oscillations of the sensor operating temperature during long-term experiments. We found that the response of the sensors depended almost linearly on the Pt loading (see Figure S5). Therefore, we discuss herein only data related to the Pt–SnO_2/RGO sample containing 20 wt% Pt. For comparison, the sensing properties of the pure and binary components prepared by the same procedures (pure SnO_2 nanoparticles, GO reduced in benzyl alcohol, and Pt/RGO nanocomposite) were also investigated.

Figure 3a,b shows the change in the resistance of the SnO_2/RGO and Pt–SnO_2/RGO sensors when exposed to different volume concentrations of H_2 at 50°C and the

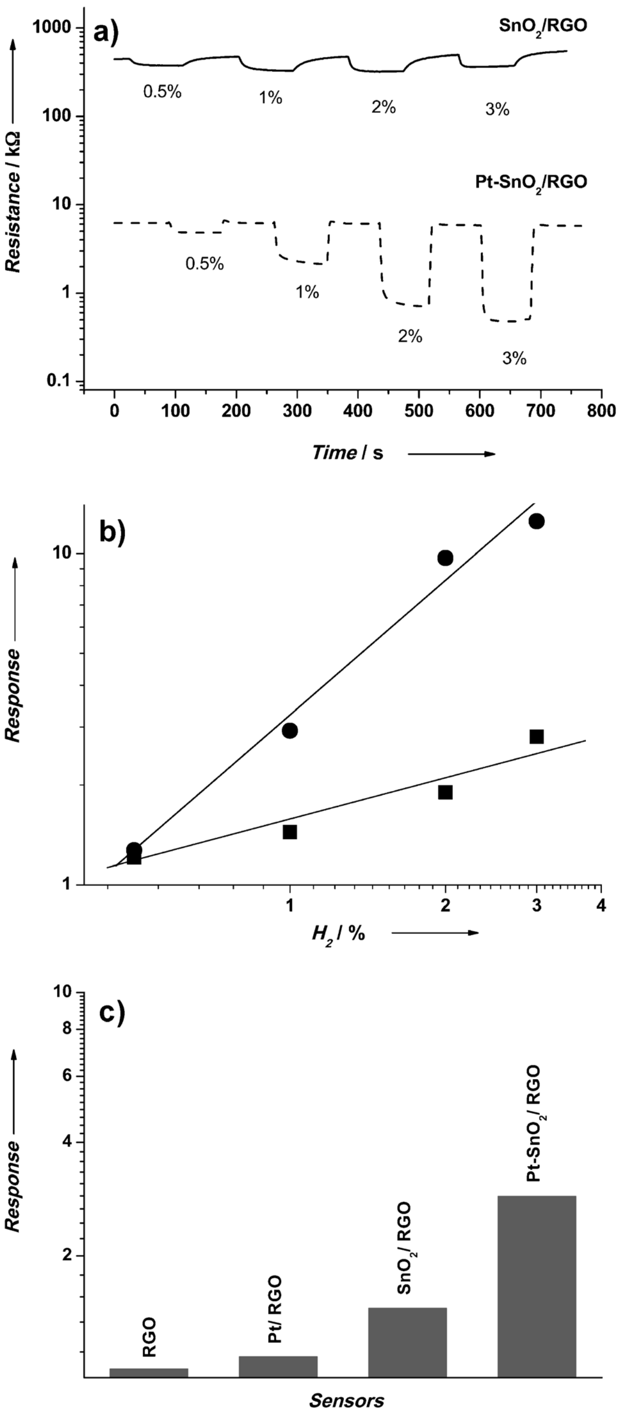

Figure 3. Hydrogen-sensing performance at 50°C of the materials investigated: a) variation in the resistance of the SnO_2/RGO (solid line) and Pt–SnO_2/RGO sensors (dashed line) with pulses of hydrogen at various concentrations (0.5, 1, 2, 3%); b) corresponding calibration curves (■ SnO_2/RGO; ● Pt–SnO_2/RGO); c) comparison of the response to 1% H_2 in air of all sensors investigated.

corresponding calibration curves; the responses to 1 % H_2 of the different sensing materials investigated are compared in Figure 3c. The pure SnO_2 nanoparticles have an extremely high resistance. In fact, at temperatures below 100 °C, the resistance of pure SnO_2 was above the detection limit of our equipment (up to ca. 10^8 Ω), and consequently the response of the SnO_2 sensor at 50 °C could not be determined and is not shown in Figure 3c. The response of the bare RGO sensor to 1 % H_2 was relatively small (Figure 3c). It is well-documented that pure graphene is not sensitive to hydrogen at low temperatures owing to the small binding energy between the hydrogen molecules and the graphene surface.[27,28,30] However, defects and functional groups present on the graphene surface act as high-energy adsorption sites for the gas molecules and can increase the sensitivity of the material.[25,38] Therefore, the response observed with the bare RGO can be attributed to the residual amount of epoxide and carboxylic groups that remain on the surface after reduction by benzyl alcohol (see Figure S6 for the FTIR characterization of this and the other sensors studied). Despite the presence of some high-energy sites, the RGO sensitivity is still quite low, which indicates that the overall interaction of the H_2 molecules with the RGO surface is very weak. These results confirm the limitations of the pure components to act as hydrogen sensors at near room temperature. As expected on the basis of previous reports on the hydrogen-sensing performance of graphene layers functionalized with metal nanoparticles,[20,23,24,26] the sensitivity of the Pt/RGO sensor is higher than that of the bare RGO. The increased response is a consequence of the catalytic action of the Pt nanoparticles in the dissociation of the hydrogen molecules.[23,24] Nevertheless, this sensor is still less sensitive than the nanostructures containing SnO_2, which show significantly higher responses to 1 % H_2 at near room temperature.

Dispersion of the SnO_2 nanoparticles on the RGO surface led to a decrease in the resistance of the composite relative to that of the pure SnO_2 (see Figure S7). This result suggests that the electrical conduction between SnO_2 grains is favored by the presence of the graphene sheets. As a consequence, measurable changes in the resistance of the composite were observed upon exposure to hydrogen gas at near room temperature, whereas traditional SnO_2-based sensors usually operate at temperatures well above 200 °C.[6] On the other hand, 1D SnO_2 nanostructures have been shown to be sensitive at room temperature; however, the response/recovery time is in the range of 2–6 min.[11]

Of all the materials tested, Pt–SnO_2/RGO exhibited the best H_2-sensing performance, with high responses to hydrogen concentrations between 0.5 and 3 % (Figure 3a,b). The sensor response clearly tracks the change in the H_2 concentration. Moreover, the responses are extremely fast, and the sensor can fully recover in very short times after hydrogen removal. Specifically, the response times, defined as the time necessary to reach 90 % of the maximum response, range between 3 and 7 s and decrease as the H_2 concentration is increased. The recovery times (time necessary for the response to decrease by 90 % from its maximum value) were in the range of 2–6 s and decreased as the H_2 concentration decreased. The sensor responses were stable and reproducible for repeated testing cycles. The remarkably higher response registered in the presence of platinum can be attributed to the catalytic role of the Pt nanoparticles in promoting the dissociation of molecular hydrogen at low temperature on the sensing layer. Indeed, the doping of semiconductor thin films with metals (Au, Pd, or Pt) that promote the catalytic decomposition of hydrogen is a well-known strategy for increasing the sensitivity of the films (a discussion on the influence of the textural properties of the composite materials on the sensing behavior is given in the Supporting Information).[39]

We also evaluated the response of the sensors to some reducing (CO, methane) and oxidizing (NO_2) interferent gases. Under the operative conditions adopted, all sensors were almost insensitive to reducing gases (see Figure S8). A strong cross-sensitivity to NO_2 was instead registered for the binary SnO_2/RGO sensor. Interestingly, the presence of Pt in the Pt–SnO_2/RGO composite led to a decrease in the response to NO_2 but enhanced the response to hydrogen and thus created a highly selective hydrogen sensor (the cross-sensitivity to humidity is discussed in the Supporting Information).

The Pt–SnO_2/RGO sensor described herein, while still highly sensitive to hydrogen concentrations of 3 % and lower, exhibited shorter response and recovery times than those found for previously reported resistive hydrogen sensors based on graphene (most of which consist of graphene-based materials functionalized with Pd or Pt; see Table 1 in the Supporting Information).[20,22–26,40,41] For example, most previously reported resistive graphene-based hydrogen sensors have response times of several minutes.[20–25,40,41] The performance of the Pt–SnO_2/RGO nanostructure in hydrogen sensing is also improved in terms of the operating temperature,[12,42] sensitivity, and noise level,[13,14,42–44] or response and recovery times,[9,13,14,42–44] relative to that of nanostructures based on SnO_2 and carbon nanotubes or 1D metal oxides. We attribute the unique properties of our sensor to the heterojunction formed between the n-type SnO_2 and p-type reduced graphene oxide in the heterostructure and the catalytic effect of Pt in promoting the dissociation of H_2 (see the complete discussion on the sensing mechanism in the Supporting Information). The catalytic role of Pt has also been assessed on the basis of the results obtained for Pt–SnO_2/RGO samples with different platinum loadings (see Figure S5).

In conclusion, we have fabricated new hydrogen sensors based on tin oxide/reduced graphene oxide and platinum/tin oxide/reduced graphene oxide heteronanostructures by extremely simple microwave-assisted routes. The sensors showed improved performance at low temperature relative to that of the corresponding pure and binary systems. In particular, the Pt–SnO_2/RGO sensor exhibited very high responses to hydrogen at concentrations between 0.5 and 3 % in air at near room temperature, with response and recovery times of 3–7 and 2–6 s, respectively. We suggest that the sensing properties of the nanocomposites are related to the heterojunction barrier formed at the SnO_2/RGO heterostructure interface. The presence of Pt, which acts as a catalytic promoter, further strongly increases the sensitivity of the SnO_2/RGO composite. Moreover, the approaches used to fabricate the sensors are extremely versatile and enable the preparation of a wide variety of metal oxides or metal nanoparticles, so that nanostructures based on different metal oxides and metals can be explored for the production of hydrogen sensors and for other applications in the field of catalysis that are currently being investigated by our research group.

Received: June 6, 2012
Revised: August 24, 2012

Keywords: hydrogen sensing · nanoparticles · platinum · reduced graphene oxide · tin oxide

---

[1] M. Balat, *Int. J. Hydrogen Energy* **2008**, *33*, 4013 – 4029.
[2] T. Hübert, L. Boon-Brett, G. Black, U. Banach, *Sens. Actuators B* **2011**, *157*, 329 – 352.
[3] H. Gu, Z. Wang, Y. Hu, *Sensors* **2012**, *12*, 5517 – 5550.
[4] H. Huang, H. Gong, C. L. Chow, J. Guo, T. J. White, M. S. Tse, O. K. Tan, *Adv. Funct. Mater.* **2011**, *21*, 2680 – 2686.
[5] S. Shao, X. Qiu, D. He, R. Koehn, N. Guan, X. Lu, N. Bao, C. A. Grimes, *Nanoscale* **2011**, *3*, 4283 – 4289.
[6] W. Göpel, K. D. Schierbaum, *Sens. Actuators B* **1995**, *26*, 1 – 12.
[7] Z. Wang, Y. Hu, W. Wang, X. Zhang, B. Wang, H. Tian, Y. Wang, J. Guan, H. Gu, *Int. J. Hydrogen Energy* **2012**, *37*, 4526 – 4532.
[8] A. Kolmakov, D. O. Klenov, Y. Lilach, S. Stemmer, M. Moskovits, *Nano Lett.* **2005**, *5*, 667 – 673.
[9] L. C. Tien, P. W. Sadik, D. P. Norton, L. F. Voss, S. J. Pearton, H. T. Wang, B. S. Kang, F. Ren, J. Jun, J. Lin, *Appl. Phys. Lett.* **2005**, *87*, 222106.
[10] E. Şennik, Z. Çolak, N. Kılınç, Z. Z. Öztürk, *Int. J. Hydrogen Energy* **2010**, *35*, 4420 – 4427.
[11] Y. Wang, X. Jiang, Y. Xia, *J. Am. Chem. Soc.* **2003**, *125*, 16176 – 16177.
[12] J. Gong, J. Sun, Q. Chen, *Sens. Actuators B* **2008**, *130*, 829 – 835.
[13] G. Lu, L. E. Ocola, J. Chen, *Adv. Mater.* **2009**, *21*, 2487 – 2491.
[14] S. Mao, S. Cui, K. Yu, Z. Wen, G. Lu, J. Chen, *Nanoscale* **2012**, *4*, 1275 – 1279.
[15] L. De Luca, A. Donato, S. Santangelo, G. Faggio, G. Messina, N. Donato, G. Neri, *Int. J. Hydrogen Energy* **2012**, *37*, 1842 – 1851.
[16] L. Renard, H. Elhamzaoui, B. Jousseaume, T. Toupance, G. Laurent, F. Ribot, H. Saadaoui, J. Brötz, H. Fuess, R. Riedeld, A. Gurlo, *Chem. Commun.* **2011**, *47*, 1464 – 1466.
[17] a) J. Villatoro, D. Monzón-Hernández, *Opt. Express* **2005**, *13*, 5087 – 5092; b) D. J. Sirbuly, S. E. Létant, T. V. Ratto, *Adv. Mater.* **2008**, *20*, 4724 – 4727.
[18] a) I. Eisele, T. Doll, M. Burgmair, *Sens. Actuators B* **2001**, *78*, 19 – 25; b) K. Scharnagl, A. Karthigeyan, M. Burgmair, M. Zimmer, T. Doll, I. Eisele, *Sens. Actuators B* **2001**, *80*, 163 – 168.
[19] a) K. Domanský, D. L. Baldwin, J. W. Grate, T. B. Hall, J. Li, M. Josowicz, J. Janata, *Anal. Chem.* **1998**, *70*, 473 – 481; b) J. Janata, M. Josowicz, *Anal. Chem.* **1998**, *70*, 179R – 208R.
[20] A. Kaniyoor, R. I. Jafri, T. Arockiadoss, S. Ramaprabhu, *Nanoscale* **2009**, *1*, 382 – 386.
[21] M. Shafiei, P. G. Spizzirri, R. Arsat, J. Yu, J. du Plessis, S. Dubin, R. B. Kaner, K. Kalantar-zadeh, W. Wlodarski, *J. Phys. Chem. C* **2010**, *114*, 13796 – 13801.
[22] J. L. Johnson, A. Behnam, S. J. Pearton, A. Ural, *Adv. Mater.* **2010**, *22*, 4877 – 4880.
[23] H. Vedala, D. C. Sorescu, G. P. Kotchey, A. Star, *Nano Lett.* **2011**, *11*, 2342 – 2347.
[24] A. Kaniyoor, S. Ramaprabhu, *Carbon* **2011**, *49*, 227 – 236.
[25] L.-S. Zhang, W. D. Wang, X.-Q. Liang, W.-S. Chu, W.-G. Song, W. Wang, Z.-Y. Wu, *Nanoscale* **2011**, *3*, 2458 – 2460.
[26] R. Kumar, D. Varandani, B. R. Mehta, V. N. Singh, Z. Wen, X. Feng, K. Müllen, *Nanotechnology* **2011**, *22*, 275719.
[27] U. Lange, T. Hirsch, V. M. Mirsky, O. S. Wolfbeis, *Electrochim. Acta* **2011**, *56*, 3707 – 3712.
[28] W. Wu, Z. Liu, L. A. Jauregui, Q. Yu, R. Pillai, H. Cao, J. Bao, Y. P. Chen, S.-S. Pei, *Sens. Actuators B* **2010**, *150*, 296 – 300.
[29] K. R. Ratinac, W. Yang, S. P. Ringer, F. Braet, *Environ. Sci. Technol.* **2010**, *44*, 1167 – 1176.
[30] R. S. Sundaram, C. Gómez-Navarro, K. Balasubramanian, M. Burghard, K. Kern, *Adv. Mater.* **2008**, *20*, 3050 – 3053.
[31] F. Favier, E. C. Walter, M. P. Zach, T. Benter, R. M. Penner, *Science* **2001**, *293*, 2227 – 2231.
[32] W. S. Hummers, R. E. Offeman, *J. Am. Chem. Soc.* **1958**, *80*, 1339 – 1339.
[33] S. Baek, S.-H. Yu, S.-K. Park, A. Pucci, C. Marichy, D.-C. Lee, Y.-E. Sung, Y. Piao, N. Pinna, *RSC Adv.* **2011**, *1*, 1687 – 1690.
[34] a) J. H. Ba, J. Polleux, M. Antonietti, M. Niederberger, *Adv. Mater.* **2005**, *17*, 2509 – 2512; b) P. Makowski, R. Rothe, A. Thomas, M. Niederberger, F. Goettmann, *Green Chem.* **2009**, *11*, 34 – 37.
[35] M. Niederberger, G. Garnweitner, *Chem. Eur. J.* **2006**, *12*, 7282 – 7302.
[36] P. Lian, X. Zhu, S. Liang, Z. Li, W. Yang, H. Wang, *Electrochim. Acta* **2010**, *55*, 3909 – 3914.
[37] D. R. Dreyer, S. Murali, Y. Zhu, R. S. Ruoff, C. W. Bielawski, *J. Mater. Chem.* **2011**, *21*, 3443 – 3447.
[38] J. T. Robinson, F. K. Perkins, E. S. Snow, Z. Wei, P. E. Sheehan, *Nano Lett.* **2008**, *8*, 3137 – 3140.
[39] A. Cabot, A. Diéguez, A. Romano-Rodríguez, J. R. Morante, N. Bârsan, *Sens. Actuators B* **2001**, *79*, 98 – 106.
[40] B. H. Chu, J. Nicolosi, C. F. Lo, W. Strupinski, S. J. Pearton, F. Ren, *Electrochem. Solid-State Lett.* **2011**, *14*, K43 – K45.
[41] L. Al-Mashat, K. Shin, K. Kalantar-zadeh, J. D. Plessis, S. H. Han, R. W. Kojima, R. B. Kaner, D. Li, X. Gou, S. J. Ippolito, W. Wlodarski, *J. Phys. Chem. C* **2010**, *114*, 16168 – 16173.
[42] M. Yang, D.-H. Kim, W.-S. Kim, T. J. Kang, B. Y. Lee, S. Hong, Y. H. Kim, S.-H. Hong, *Nanotechnology* **2010**, *21*, 215501.
[43] H. T. Wang, B. S. Kang, F. Ren, L. C. Tien, P. W. Sadik, D. P. Norton, S. J. Pearton, J. Lin, *Appl. Phys. Lett.* **2005**, *86*, 243503.
[44] F. Rumiche, H. H. Wang, J. E. Indacochea, *Sens. Actuators B* **2012**, *163*, 97 – 106.